Fermi National Accelerator Laboratory

FERMILAB-Pub-92/245-E

Measurement of the J/ψ and ψ' Resonance Parameters in $\bar{p}p$ Annihilation

T.A. Armstrong *et al.*

(The E760 Collaboration)

Fermi National Accelerator Laboratory, Batavia, Illinois 60510

September 1992

Submitted to *Physical Review D*

Operated by Universities Research Association Inc. under Contract No. DE-AC02-76CHO3000 with the United States Department of Energy

Disclaimer

FERMILAB-Pub-92/245-E

Measurement of the J/ψ and ψ' Resonance Parameters in $\bar{p}p$ Annihilation

T.A.Armstrong[6], D. Bettoni[2], V. Bharadwaj[1], C. Biino[7], G. Borreani[2], D. Broemmelsiek[4], A. Buzzo[3], R. Calabrese[2], A. Ceccucci[7], R. Cester[7], M.D. Church[1], P. Dalpiaz[2], P.F. Dalpiaz[2], R. Dibenedetto[7], D. Dimitroyannis[5], M.G. Fabbri[2], J.E. Fast[4], A. Gianoli[2], C.M. Ginsburg[5], K.E. Gollwitzer[4], A.A. Hahn[1], M.A. Hasan[6], S.Y. Hsueh[1], R.A. Lewis[6], E. Luppi[2], M. Macrí[3], A. Majewska[6], M.A. Mandelkern[4], F. Marchetto[7], M. Marinelli[3], J.L. Marques[4], W. Marsh[1], M. Martini[2], M. Masuzawa[5], E. Menichetti[7], A. Migliori[7], R. Mussa[7], S. Palestini[7], M. Pallavicini[3], S. Passaggio[3], N. Pastrone[7], C. Patrignani[3], J. Peoples, Jr.[1], L. Pesando[7], F. Petrucci[2], M.G. Pia[3], S. Pordes[1], P.A. Rapidis[1], R.E. Ray[5*], J.D. Reid[6], G. Rinaudo[7], B. Roccuzzo[7], J.L. Rosen[5], A. Santroni[3], M. Sarmiento[5], M. Savrié[2], A. Scalisi[3], J. Schultz[4], K.K. Seth[5], A. Smith[4], G.A. Smith[6], M. Sozzi[6], L. Tecchio[7], S. Trokenheim[5], M.F. Weber[4], S.J. Werkema[1], Y. Zhang[6], J.L. Zhao[5], G. Zioulas[4], M. Zito[3†].

(E-760 Collaboration)

[1] *Fermi National Accelerator Laboratory, Batavia, Illinois 60510*
[2] *I.N.F.N. and University of Ferrara, I-44100 Ferrara, Italy*
[3] *I.N.F.N. and University of Genoa, I-16146 Genoa, Italy*
[4] *University of California at Irvine, California 92717*
[5] *Northwestern University, Evanston, Illinois 60208*
[6] *Pennsylvania State University, University Park, Pennsylvania 16802*
[7] *I.N.F.N. and University of Turin, I-10125 Turin, Italy*

We report new measurements for the mass, width, and branching ratios for the J/ψ and the ψ'. These charmonium states are formed exclusively in $\bar{p}p$ annihilations at the Fermilab Antiproton Accumulator ring, where stochastically cooled antiprotons are brought into collision with the protons of an internal hydrogen gas jet target. The antiproton energy is precisely controlled and measured allowing an accurate measurement of the resonance parameters. From the shape of the excitation curves we find that the widths of J/ψ and ψ' are $\Gamma(J/\psi) = 99 \pm 12 \pm 6$ keV and $\Gamma(\psi') = 306 \pm 36 \pm 16$ keV, and that the mass of the J/ψ is $3096.87 \pm 0.03 \pm 0.03$ MeV/c^2. For the J/ψ we obtain $B(J/\psi \to \bar{p}p)\ B(J/\psi \to e^+e^-) = (1.14^{+0.16}_{-0.12} \pm 0.10) \times 10^{-4}$; for the ψ' we obtain $B(\psi' \to \bar{p}p)\ [B(\psi' \to e^+e^-) + B(\psi' \to J/\psi X)B(J/\psi \to e^+e^-)] = (1.17^{+0.14}_{-0.12} \pm 0.08) \times 10^{-5}$.

PACS numbers : 14.40.Gx, 29.20.Dh

I. INTRODUCTION

To date the majority of the measurements of the J/ψ and ψ' resonance parameters are the result of experiments carried out with e^+e^- colliding beams[1]. The mass determination from such experiments is very precise[2], but the resonance width measurements are compromised by the relatively large beam energy spread and the large radiative corrections[1]. Charmonium states can also be formed in $\bar{p}p$ annihilations, where they can be easily detected, despite the presence of a much larger hadronic background, by their characteristic decays into final states with a high mass e^+e^- pair. Moreover, the small energy spread of stochastically cooled antiprotons and the precise control of the beam energy available at an antiproton storage ring provide a high precision probe for the determination of the mass and width of narrow resonances[3].

A significant advantage of the study of charmonium in $\bar{p}p$ collisions is that the full spectrum of states can be resonantly produced, in contrast to e^+e^- annihilations where only states with the quantum numbers of the photon ($J^{PC} = 1^{--}$) are directly accessible. This makes the direct study of the χ_c states and searches for previously unobserved states, such as $h_c(^1P_1)$, feasible[4].

In the present experiment, Fermilab E760, circulating antiprotons in the Fermilab Antiproton Accumulator are brought into collision with an internal hydrogen gas jet target[5]. A non-magnetic detector identifies the charmonium final states by detecting their electromagnetic decays. Data collected during two periods (July through August, 1990, and August through December, 1991) with typical luminosities of 5×10^{30} $\mathrm{cm}^{-2}\mathrm{s}^{-1}$ are used to obtain the results reported here. The momentum spread $\Delta p/p$ of the beam is less than 2×10^{-4} which leads to FWHM resolution of approximately 0.5 MeV in the center of mass energy.

The present experiment is similar to a previous CERN ISR experiment[6] but offers substantial improvements in beam quality, luminosity, and detector equipment. We report new measurements for the mass, width, and branching ratios for the J/ψ and the ψ', and the techniques used in obtaining these results.

II. EXPERIMENTAL TECHNIQUE

The charmonium states are studied by sweeping the $\bar{p}$ energy across the resonances and measuring their cross sections as a function of the beam energy; the resonance parameters are extracted by an analysis of the resulting excitation curve. The Breit-Wigner cross section for the formation and subsequent decay of a $c\bar{c}$ resonance R of spin J, mass M_R, and total width Γ_R formed in the reaction $p\overline{p} \rightarrow R$ is

$$\sigma_{BW}(E_{cm}) = \frac{(2J+1)}{(2S+1)(2S+1)} \frac{4\pi(\hbar c)^2}{(E_{cm}^2 - 4(m_p c^2)^2)} \times \frac{\Gamma_R^2 B_{in} B_{out}}{(E_{cm} - M_R c^2)^2 + \Gamma_R^2/4} \quad . \tag{1}$$

Here S is the spin of the proton, B_{in} and B_{out} are the branching ratios ($B = \Gamma_{partial}/\Gamma_R$) in the resonance formation channel ($\bar{p}p \rightarrow R$) and in the decay channel respectively. For the present study we select the decay channels $R \rightarrow e^+e^-$, or $R \rightarrow e^+e^-X$ where the e^+e^- pair forms either a J/ψ or a ψ'. The center-of-mass energy E_{cm} is determined only from the $\bar{p}$ beam energy E. The observed excitation curve is the convolution of the Breit-Wigner cross section for the resonance with the energy distribution function of the beam, i.e.,

$$\sigma(E_{cm}) = \int_0^\infty \sigma_{BW}(E')G(E' - E_{cm})\,dE', \tag{2}$$

where $G(E)$ is the normalized beam energy distribution function in the center of mass frame. The area under the resonance is given by

$$A = \int_0^\infty \sigma(E_{cm})dE_{cm} = \frac{\pi}{2}\sigma_{peak}\Gamma_R, \tag{3}$$

which is independent of the form of $G(E)$. σ_{peak} is the cross section at $E_{cm} = M_Rc^2$ given by

$$\sigma_{peak} = \frac{(2J+1)}{(2S+1)(2S+1)}\frac{16\pi\hbar^2 B_{in}B_{out}}{(M_R^2 - 4m_p^2)c^2} \quad . \tag{4}$$

If $G(E)$ is unknown, then the product $\sigma_{peak}\Gamma_R$ can be obtained from the measured area. If $G(E)$ is known, then Γ_R can be directly determined from the analysis of the shape of the measured excitation function. The precision with which the width Γ_R can be extracted depends on the relative magnitudes of Γ_R and the beam width Γ_B (FWHM) in the center of mass. If $\Gamma_R/\Gamma_B > 1$, Γ_R can be determined with good precision; the precision decreases as Γ_R/Γ_B decreases.

With our beam width, $\Gamma_B \approx 500$ keV, a direct determination of Γ_R can be made from the analysis of the shape of the resonance excitation function even for the J/ψ resonance ($\Gamma_R \approx 100$ keV). One can understand the reason for our sensitivity to such small resonance widths from the following considerations. For a beam energy distribution that is a Gaussian with width $\Gamma_B(= (8\ln 2)^{1/2}\sigma_B)$, the measured peak cross section σ^*_{peak} is

$$\sigma^*_{peak} = \sigma_{peak}\sqrt{\frac{\pi}{8}}\,\frac{\Gamma_R}{\sigma_B}\,\exp\left(\frac{\Gamma_R^2}{8\sigma_B^2}\right)\,\mathrm{erfc}\left(\frac{\Gamma_R}{\sqrt{8}\sigma_B}\right)\,, \tag{5}$$

where erfc is the complementary error function. If $\Gamma_B > \Gamma_R$ it can be shown that

$$\frac{\sigma^*_{peak}}{A} \simeq \frac{0.94}{\Gamma_B}\left[1 - 0.94\frac{\Gamma_R}{\Gamma_B}\right], \tag{6}$$

where 0.94 is the factor $(4\ln 2/\pi)^{1/2}$. In our case Γ_R/Γ_B is ≈ 0.2 at the J/ψ and a direct determination of Γ_R can be obtained if σ^*_{peak}/A is measured. We would like to note that if we had a resonance cross section with a Gaussian shape and a Gaussian beam energy distribution we would have instead

$$\frac{\sigma^*_{peak}}{A} \simeq \frac{0.94}{\Gamma_B}\left[1-\frac{1}{2}\left(\frac{\Gamma_R}{\Gamma_B}\right)^2\right], \tag{7}$$

i.e., a much weaker dependence on Γ_R/Γ_B than that of Eq. (6) for a Breit-Wigner resonance cross section. It is this fact that allows an accurate determination of Γ_R.

We also wish to point out that the ratio σ^*_{peak}/A is independent of the efficiency and acceptance of the detector and the absolute value of the luminosity, and Γ_R can be determined without having a detailed knowledge of these quantities. Stable running conditions, an accurate knowledge of the beam energy distribution function, and high statistical accuracy in the data are, however, necessary.

III. THE ANTIPROTON ACCUMULATOR

The Fermilab Antiproton Accumulator is a storage ring designed to accumulate and cool antiprotons for the Tevatron colliding beam program[7]. The 474 meter ring was originally designed to operate at a fixed total energy of 8.9 GeV. In order to provide antiprotons over a range of 4–7 GeV (Table I) for use in the present experiment, the Accumulator is operated in a non-standard mode. In the following we briefly describe the important features of the machine.

The Accumulator lattice consists of six identical sectors. The lattice functions and the plan view of a sector are shown in Fig. 1. The ring is completed with mirror symmetry about the point at which two sectors are joined. As shown by the dot-dash line in the figure, the momentum dispersion of a sector starts from 0 m at one end and increases to 9 m at the other end. The experiment is located at a zero dispersion region where the horizontal and vertical betatron functions (solid and dashed lines in Fig. 1) are the same; i.e., the transverse beam profile is circular at the interaction region.

During the experiment, the Accumulator is run first in its design mode to accumulate the desired number of antiprotons at 8.9 GeV. Then the $\bar{p}$ beam is decelerated to the desired energy[8]. An RF cavity operating at the second harmonic of the beam revolution frequency ($f_{RF} \approx 1.24$MHz) and with a maximum RF voltage amplitude of 3 kV is used to decelerate the beam. The deceleration process is controlled by an auxiliary front-end computer[9] that sets the current of magnets as a function of beam momentum. These functions, or "ramps," are determined experimentally at discrete points and interpolated linearly between the points. The deceleration proceeds at about 20 MeV/s. After the deceleration, the resonance is scanned by changing the beam energy in small steps. The smallest step size is determined by the least significant bit of the dipole power supply digital control and corresponds to about 150 keV/c in the lab. The main dipole and quadrupole power supplies are regulated to 1 part in 10^5 to ensure excellent stability of the beam orbit and energy.

In a typical run for the present experiment, a beam of $\approx 3.5 \times 10^{11}$ antiprotons is accumulated at an average rate of $\approx 10^{10}\,\bar{p}$/hr. The internal hydrogen gas jet target is operated at a typical density of 3.5×10^{13} atoms/cm^2. It has a diameter of 6.3 mm

in the interaction region (for 95% containment). The antiproton beam has a diameter of $\approx$ 5 mm (for 95% containment) and traverses the gas jet at $\approx$0.62 MHz. The peak luminosity achieved is $\approx 1.0 \times 10^{31}$ cm^{-2}s^{-1}. The beam lifetime is 50 to 90 hours depending on the energy of the beam. Each store is used for about 1–2 lifetimes. In the case of the J/ψ and the ψ' the relatively high production cross sections allow us to complete an energy scan of a resonance within a single store.

The stochastic cooling system[10] is essential to the success of this experiment. The transverse cooling system counteracts the growth of beam emittance due to the traversals of the gas jet and the residual gas in the ring. The momentum cooling serves two purposes: it compensates for the average dE/dx loss due to the beam traversing the jet and it narrows the beam energy spread Γ_B to $\approx$ 0.5 MeV in the center of mass. A set of movable momentum cooling pick-up electrodes[11] allows us to cool the beam at any radial orbit position and lets us choose the beam orbit position.

IV. BEAM ENERGY AND WIDTH MEASUREMENTS

The average beam energy and the beam energy spread are important for the determination of the mass and width. The precision of the beam energy measurement determines the precision of the measurement of the resonance mass. The precision with which the beam energy width is measured directly influences how well the resonance width of a narrow resonance can be determined. We describe here how these quantities are determined.

A. Introduction

The determination of the average beam energy and the beam energy spread are both based on the measurement of the beam revolution frequency spectrum. The beam energy in the lab is determined from the velocity of the beam. The beam velocity is given by:

$$c\beta = fL \ , \tag{8}$$

where f is the revolution frequency of the particles in the beam and L is the orbit length. L is usually expressed as the sum of a reference orbit length L_0 and a difference ΔL, i.e.,

$$L = L_0 + \Delta L \ . \tag{9}$$

The energy spread of the beam is derived from the revolution frequency spread of the beam. From Eq. (8) we get

$$\frac{df}{f} = \frac{d\beta}{\beta} - \frac{dL}{L}. \tag{10}$$

In terms of the beam momentum p,

$$\frac{d\beta}{\beta} = \frac{1}{\gamma^2}\frac{dp}{p} \ . \tag{11}$$

The transition gamma γ_t is defined by

$$\frac{dL}{L} = \frac{1}{\gamma_t^2}\frac{dp}{p} \ . \tag{12}$$

The value of γ_t depends on the machine lattice. From Eqs. (10), (11), and (12) we have the following relationship between the fractional momentum spread dp/p and the fractional frequency spread df/f:

$$\frac{dp}{p} = \frac{1}{\eta}\frac{df}{f}, \tag{13}$$

where η is defined as:

$$\eta \equiv \frac{1}{\gamma^2} - \frac{1}{\gamma_t^2}. \tag{14}$$

The beam revolution frequency spectrum is measured from the beam current Schottky noise[12]. The spectral power density $P(f)$ of the noise is proportional to the particle density dN/df, i.e.,

$$P(f)\Delta f = 2\pi(ef)^2\frac{dN}{df}\Delta f \ , \tag{15}$$

where e is the charge of the antiproton. A spectrum at the 129th harmonic of the revolution frequency is shown in Fig. 2. The signal is detected by a coaxial quarter wavelength resonant pick-up whose bandwidth is much larger than the beam frequency width (f_{PU} = 79.323 MHz, Q_{PU} = 305). The signal is analyzed by a spectrum analyzer[13] every 3 to 5 minutes; the spectrum is then read out by the experiment data acquisition system. As shown in Fig. 2 the average revolution frequency spectrum is approximately Gaussian in shape with a tail on the low-energy side caused by straggling primarily in the gas-jet target. This spectrum is fitted to a curve, converted to the corresponding center-of-mass energy spectrum, and used as the energy distribution function $G(E)$ which is convoluted with the Breit-Wigner cross section in Eq. (2).

B. Orbit length measurement

The length of the central orbit obtained from survey measurements is not accurate enough to determine the beam energy with sufficient precision to improve on the existing measurements of the J/ψ and ψ' masses[2][14]. We have therefore chosen to calibrate the orbit length with the known mass of the ψ'.

The reference orbit length at the peak of the resonance is given by $L_0 = c\beta_0/f_0$, where f_0 is measured at this orbit, and β_0 is calculated from the ψ' mass. The error δL_0 in the length of the reference orbit and the error in the reference mass δM_R are related by the equation

$$\frac{\delta L_0}{L_0} = \frac{M_R}{\gamma_0^3 \beta_0^2 m_p^2} \delta M_R, \tag{16}$$

where we have neglected the contribution of the error in the average beam frequency which is small ($\delta f_0/f_0 = \pm 1.5 \times 10^{-7}$). The ± 0.1 MeV/c^2 uncertainty in the published[14] mass of the ψ' corresponds to an uncertainty in the L_0 of ± 0.67 mm at the ψ'. An orbit length error of ± 0.67 mm corresponds to δM_R= 0.033 MeV/c^2 at the J/ψ.

Having established the reference orbit at the ψ', we can determine the center-of-mass energy at the other resonances. If we could keep the beam on the reference orbit at all energies the only error in a resonance mass would be that discussed above. However, this situation cannot be achieved precisely over the entire energy range of the experiment. In general orbits used differ in length from the reference orbit by an amount ΔL which typically ranges from +2 mm to -2 mm.

The difference ΔL is measured using 48 horizontal beam position monitor (BPM) modules[15] located near the horizontally focusing quadrupoles of the accumulator lattice (see Fig. 1). The BPM readout at the energy of interest is compared to the BPM readout that has been recorded at the reference energy. The resulting "difference orbit" is used to calculate ΔL.

The orbit length change, expressed in terms of the difference $\Delta x(s)$ in the horizontal position between the reference orbit and the current orbit is given to first order by:

$$\Delta L = \int_0^{L_0} \frac{\Delta x(s)}{\rho(s)} ds, \tag{17}$$

where $\rho(s)$ is the radius of curvature of the reference orbit at position s, along the path of the reference orbit. The higher-order terms not appearing in Eq. (17) turn out to be of the order of 10^{-4} of the first order term. Orbit length changes due to variations in the vertical position of the beam are also negligible. Since

$$\rho(s)^{-1} = \frac{eB(s)}{p} \tag{18}$$

and the magnetic field B is large only in the dipole magnets, we can approximate the integral of Eq. (17) by a sum which includes only the contribution of the 30 main bending dipole magnets:

$$\Delta L = \sum_{i=1}^{30} \frac{\Delta \mathrm{x}_i}{\rho} \Delta s_i, \tag{19}$$

where $\Delta \mathrm{x}_i$ is the horizontal displacement from the reference orbit at the center of the ith dipole, ρ is the radius of curvature of the main dipoles (17.464 m), and Δs_i is the effective length of the ith dipole.

Eq. (19) requires that Δx_i be known at the center of each dipole magnet. We calculate them from a fit to the closed orbit formula[16] using the 48 BPM measurements. The error in the orbit length measurement is calculated to be ± 1 mm using a Monte Carlo method; in this calculation we assign a random error to the BPM readouts equal to the statistical error for each BPM detector ($1/\sqrt{12}$ of the least significant bit). We have checked this by using BPM data from the double scans (see section IV C 1) in which the cooling pick-up positions and the cooling gain were very well controlled. The orbit length at each data point in these scans can be assumed to be constant and the length differences calculated from the BPM measurements are simply due to statistical fluctuations. Another method to check the BPM error is given in section VII A. We conclude that the orbit length error is ± 1 mm, consistent with the hypothesis that the error is statistical only. The corresponding mass errors are δM_R=0.05 MeV/c^2 at the J/ψ and δM_R=0.15 MeV/c^2 at the ψ'.

C. Beam energy spread measurement

The beam energy spectrum is determined from the beam revolution frequency spectrum. It is therefore important to determine dE/df, or equivalently the η parameter of Eq. (14). In the following, we describe three methods to determine η.

1. Determination of η by the double scan technique

In a double scan, we scan the resonance twice, once with the beam on the "central orbit" and another time on a "side orbit." The side orbit is radially displaced from the central orbit. The frequency difference between the two orbits is chosen to be about one σ_f of the beam frequency spread. If we know the energy difference between the two orbits, dE/df can be readily calculated. Since the peak of the resonance defines the energy of the beam uniquely, we can use it as a marker to measure the energy difference between the two orbits.

The double scan procedure is schematically illustrated in Fig. 3. The sequence of data taking is indicated by the arrows shown. Data are first taken with the beam on the central orbit, with the revolution frequency, total energy, and the magnetic field B being (f_c, E_c, B_c). The beam is decelerated from the central to the side orbit, where more data are taken. The energy and frequency of the beam change but the B-field is the same: $(f_s, E_s, B_s = B_c)$. The beam is then returned to the central orbit by changing the B-field but keeping the energy constant; and the procedure is repeated several times across the resonance. The resulting cross section measurements can be plotted against the B-field producing two excitation curves which are shifted with respect to each other as shown in Fig. 3.

To obtain the quantity dE/df at constant B, we now consider "sets" of points taken at the same magnetic field but on different orbits. One set consists of cross section measurements at energies E_c^i, another at energies E_s^i. The value of dE/df can be found, in essence, by forcing the excitation curve from the side orbit to match the

central orbit curve. To be more specific, consider the data points of Fig. 3. Points 2 and 3 form a set, and points 1 and 2 are the peaks of the two excitation curves. We have

$$(E_2 - E_3) = \frac{dE}{df}(f_2 - f_3), \tag{20}$$

and

$$(E_1 - E_3) = \beta^2\gamma^3 m_p \frac{(f_1 - f_3)}{f_3}. \tag{21}$$

Since E_1 and E_2 are equal, we get from Eqs. (20) and (21)

$$\frac{dE}{df} = \beta^2\gamma^3 m_p \frac{1}{f_3}\frac{(f_1 - f_3)}{(f_2 - f_3)}. \tag{22}$$

Equivalently, η, as defined in Eq. (13), is

$$\eta = \frac{1}{\gamma^2}\frac{(f_2 - f_3)}{(f_1 - f_3)}. \tag{23}$$

The derivation above assumes that the orbit length for data points 1 and 3 are exactly the same. This is in general true for adjacent points to the level of the power supply digital setting error, i.e., ± 0.027 mm, which is indeed negligible. In addition, we assume that points 1 and 2 can be determined with sufficient statistical accuracy from a fit to the two excitation curves.

We see from Eqs. (22) and (23) that dE/df or η can be measured accurately by this method because it depends only on frequency measurements; the parameters in the equations (β and γ) are known accurately because the resonance masses of J/ψ and ψ' are accurately known[2].

2. *Determination of η from the synchrotron frequency*

When the RF is on, the energy of a particle oscillates about the synchronous energy with a characteristic synchrotron frequency. The synchrotron frequency ω_s depends on η and several other machine parameters. In the small oscillation amplitude limit the relation is [16]

$$\omega_s^2 = \frac{eV_{RF}}{E}\frac{\omega_{RF}^2}{2\pi h}\frac{\eta\cos(\phi_s)}{\beta^2}, \tag{24}$$

where V_{RF} is the peak RF voltage seen by the beam, ω_{RF} is the RF frequency, the RF cavity operates at harmonic number h= 2, and ϕ_s is the synchronous phase. If the beam is stationary (neither accelerating nor decelerating) the synchronous phase ϕ_s=0 above transition ($\gamma > \gamma_t$), and $\phi_s = \pi$ below transition ($\gamma < \gamma_t$).

There are several measurements that must be made in order to evaluate η from Eq. (24). The energy of the beam is known to better than 1 part in 10^4 using the techniques discussed in Sec. IV B. The RF frequency is known to 1 part in 10^7. For the beam energies of interest to us, the synchrotron frequency typically varies between several Hz to several tens of Hz. By extending the measurement over many synchrotron frequency harmonics (typically 8 to 12) the synchrotron frequency can be determined to better than 1%.

The primary uncertainty in the determination of η from this technique is due to the uncertainty in the measurement of V_{RF}. The most accurate measurement of V_{RF} utilizes a bolometric RF power meter. The harmonic content of the RF voltage is measured by a spectrum analyzer. The overall uncertainty in the determination of η from this method is estimated to be approximately 10%. The results in the measurement of η by this method are listed Table II.

3. *Determination of η from γ_t measurement*

From Eq. (14), η can be determined from a knowledge of the transition gamma, γ_t. In turn, γ_t can be determined by measuring the change in revolution frequency of a beam of fixed energy (RF off) caused by the change in the magnetic field B of the main dipoles, the relation being

$$\frac{dB}{B} = \gamma_t^2 \frac{df}{f}. \tag{25}$$

Unfortunately, because

$$\frac{d\eta}{\eta} = \left[\frac{2}{\eta\gamma_t^2}\right]\frac{d\gamma_t}{\gamma_t}, \tag{26}$$

the error in η resulting from the error in γ_t approaches infinity as $\eta \to 0$. Because of this large uncertainty, the determination of η by measurements of γ_t is difficult when η is small. The error in η measured using this technique is hard to estimate, and we do not quote it or use these measurements in our analysis. The results from this method are listed in Table II only for comparison with the results from the other two methods.

V. THE E760 DETECTOR

The E760 apparatus is designed to select electromagnetic final states out of a very large hadronic background and to identify unambiguously the topology of events. A schematic of the detector, gas jet and luminosity monitor is shown in Fig. 4. The detector covers the complete azimuth and the laboratory polar angle from 2° to 70°. There are two cylindrical scintillator hodoscopes H1 and H2 used for triggering and charged particle identification. A threshold Čerenkov counter provides

electron/hadron discrimination and wire chambers provide charged particle tracking. The central calorimeter measures electron and photon energies and positions. All of the above, except the wire chambers, are also used in the trigger.

Scintillation counter hodoscope H1 consists of 8 elements of 2 mm thick plastic scintillator lining the exterior of the 0.2 mm thick stainless steel beam pipe and covers a polar angle range from 9° to 65°. A single minimum-ionizing particle yields an average of 10–20 photoelectrons in this hodoscope. The second hodoscope H2 consists of 32 counters, each 4 mm × 3 cm × 65 cm, at a radius of 17 cm from the beamline. Since the light yield in H2 is good (50–100 photoelectrons per minimum ionizing particle), the pulse height is also used to distinguish single charged particles from electron-positron pairs.

The Čerenkov counter[17] is divided into eight azimuthal sectors, each covering 45°. Within each sector there are two cells covering the polar angle from 15° to 38° and 38° to 70°, respectively. The cells are filled with CO_2 and Freon-13 at one atmosphere and have a pion momentum threshold of 4.9 GeV/c and 3.7 GeV/c, respectively.

The central calorimeter CCAL[18] consists of 1280 lead-glass blocks arranged in 20 rings in the polar coordinate θ and 64 wedges in the azimuthal coordinate ϕ in a projective geometry. Each block is instrumented with a photomultiplier whose output signal is digitized in an 11-bit ADC. In addition, summed output signals from matrices of 5×8 blocks that map the central calorimeter to a coarse $\theta - \phi$ grid are used in the fast trigger logic[19]. The root mean squared (RMS) energy resolution of this detector is $6\%/\sqrt{E(\mathrm{GeV})}$. The forward lead scintillator calorimeter[20] which covers the polar angle from 2° to 12° is not used for this analysis.

The wire chamber system covers the range of θ from 15° to 65° and consists of: a) A straw-tube drift chamber[21] made with two layers of aluminized mylar tubes, b) A radial projection drift chamber RPC[22] which samples dE/dx information 16 times for each track, and, on the same mechanical structure as the RPC, a multi-wire proportional chamber with cathode pad readout, c) a set of outer tracking chambers consisting of a cylindrical barrel of limited streamer tubes[23] for θ larger than 22°, and a planar multi-wire proportional chamber covering the range of θ from 10° to 18°. Straw-tube drift chambers covering smaller polar angles are not used in this analysis.

The overall RMS angular resolutions in the detector system are $\Delta\theta$=4 mrad and $\Delta\phi$=7 mrad for electrons, and $\Delta\theta$=7 mrad and $\Delta\phi$=11 mrad for photons.

The luminosity monitor[24] consists of a fixed 1 cm × 5 cm and 0.5 mm deep active volume surface barrier silicon detector mounted ≈1.5 m from the interaction region. It detects recoil protons elastically scattered at 86.5° from the beam direction. The luminosity $\mathcal{L}$ is determined by normalizing the recoil counts to the known elastic scattering cross section,

$$\mathcal{L} = N_{elastic}/[\frac{d\sigma_{elastic}}{d\Omega}d\Omega]. \tag{27}$$

where $d\Omega$ is the solid angle subtended by the silicon detector. The error in the absolute measurement of the luminosity is mostly due to the error in the fit to the known $p\bar{p}$

total cross sections in the 2.5-15.0 GeV/c region and the uncertainty in solid angle $d\Omega$. The error due to counting statistics makes a much smaller contribution to the overall luminosity errors, which are estimated to be less than $\pm 4\%$. An independent measurement of the relative luminosity is provided by the coincidences between H1 and H2. The ratio of the rate for these coincidences to the rate in the luminosity monitor is stable to $\pm 1.5\%$ over a scan.

VI. EVENT SELECTION AND DATA ANALYSIS

Events are selected for recording by the fast hardware trigger designed to identify a high mass object decaying to e^+e^- with no explicit condition on additional particles, charged or neutral. This choice was made in order to use the same trigger logic for all charmonium resonances decaying either inclusively to J/ψ or exclusively to e^+e^-. The elements which enter into the trigger are: logic signals from the Čerenkov cells and from the hodoscopes (H1 and H2), and the summed signals from the lead-glass counters.

Three simultaneous hardware triggers have been implemented:

1. The main trigger requires two electrons each defined by a coincidence between the appropriate elements of scintillator hodoscopes H1 and H2, and identified as an electron by the associated Čerenkov signal. Independently, two energy clusters, above their θ-dependent energy thresholds, are required in the CCAL with an azimuthal opening angle greater than 90°.

2. An auxiliary trigger requires Čerenkov electron identification for only one of the two charged particles to monitor the efficiency of the Čerenkov detector.

3. Another auxiliary trigger which does not use any information from the CCAL monitors the efficiency of this calorimeter.

The offline analysis for the J/ψ requires exactly two energy clusters in the CCAL each with θ greater than 15°. For the 1991 data, where the interaction rate was higher, we relax somewhat the two cluster requirement. During this running period the summed output signals from the CCAL used for the trigger were also read out with a shorter integration gate. This allows a classification of clusters as on-time or out-of-time with respect to the trigger. For cluster energies greater than 200 MeV we reliably classify the clusters, while for lower cluster energies we do not classify them. For the 1991 data the two cluster requirement was applied only to on-time or lower energy clusters.

The invariant mass for the two electron system is calculated as $M_{e_1e_2} = (2E_{e_1}E_{e_2}(1-\cos\theta_{12}))^{1/2}$, where E_{e_1} and E_{e_2} are the two cluster energies, and θ_{12} is the opening angle between them. The $M_{e_1e_2}$ distribution is plotted in Fig. 5, together with the background determined from running at off-resonance energies (E_{cm} = 2.911 to 3.050 GeV). The final J/ψ sample is selected by making a cut at $M_{e_1e_2} = 2.75$ GeV/c^2 to eliminate the low mass background. The efficiency ϵ_{anal} of the applied cuts has been obtained by measuring in turn the efficiency of each particular cut on a sample of clean events, obtained by tightening the requirements applied in the other

uncorrelated cuts.

For the ψ' the two cluster requirement is not appropriate because the inclusive decays $\psi' \to J/\psi + X$ have a higher multiplicity. Instead, single electrons are identified using five quantities: the amplitude of the signal from the H2 counter, the amplitude of the signal from the Čerenkov counter, the dE/dx information from the RPC and the two second moments of the transverse shower distribution in the CCAL. For each of these variables a probability distribution function for electrons is calculated from a clean sample of J/ψ events. We can then calculate the joint probability for a track to be an electron as the product of the five probabilities. Similarly, we calculate the joint probability for a track to be a hadron based on the probability distributions for the five quantities obtained from a sample of events taken at E_{cm}=3.613 to 3.667 GeV, a region far from any resonances decaying to J/ψ. Each track is then identified as an electron or a hadron based on the ratio of the electron probability to the hadron probability. The efficiency of identifying electrons in this way has been measured by studying a sample of electron tracks from fully reconstructed events coming from the reaction $\chi_{c_2} \to J/\psi\gamma \to e^+e^-\gamma$[25] and is approximately 0.9. Events with two electrons having $M_{e_1e_2}$ larger than 2.8 GeV/c^2, and θ in the 15° to 60° range for both electrons are accepted. The $M_{e_1e_2}$ distribution is shown in Fig. 6, together with the background determined from the off resonance running at 3.667 GeV. Both inclusive and exclusive e^+e^- decays of the ψ' resonance are clearly seen.

The overall efficiency ϵ is the product of the trigger efficiency ϵ_{trig}, the geometrical acceptance ϵ_{geom}, and ϵ_{anal}. The main source of trigger inefficiency is in the requirement of alignment between H1 and H2 counters, and is related to the size of the interaction volume. Using a sample of events with track multiplicity greater than 2, the efficiency of this requirement is determined to be equal to 0.87±0.02 for the data collected in 1990, and to 0.94±0.02 for 1991, the difference being due to a modification in the trigger configuration. The trigger inefficiencies related to the Čerenkov counter and to the CCAL are determined by comparing the output of the three simultaneous triggers.

The geometrical acceptance of the detector depends on the angular distribution of the e^+e^- in the final state. For the J/ψ this distribution is of the form $1 + \lambda\cos^2\theta$ where θ is measured in the J/ψ frame and $\lambda(J/\psi) = 0.63 \pm 0.08$[26] . For the ψ' the expected distribution[27] is of the form $1 + \lambda\cos^2\theta_{J/\psi}$, where $\theta_{J/\psi}$ is measured in the J/ψ rest frame. We use the approximation $\cos\theta_{J/\psi} \approx < \cos\theta >$, where $< \cos\theta >$ is the average of $|\cos\theta|$ of the two electrons measured in the ψ' frame. From a fit to our own data we determine $\lambda(\psi') = 0.69 \pm 0.26$. Using these values for λ we can determine ϵ_{geom}. The efficiencies for the four data sets are tabulated in Table III.

The data for each scan of a resonance are analyzed separately. Data for a scan are binned according to beam energy. At each of the N energy points the data consists of the frequency spectrum, the number of events, and the integrated luminosity $\mathcal{L}$.

The measured beam revolution frequency spectrum can be fitted very well over a wide range of frequencies with a "double Gaussian" function defined as two half

Gaussians joined at the peak. The width on the low-energy side is typically 10–20% wider than the high-energy side. A low energy tail due to straggling usually contains less than 0.1% of the beam. We have studied different ways of fitting the frequency spectra with more complex functional forms. The basic form is always the "double Gaussian." Depending on the scan, exponential tails or a polynomial up to 8th order may be added to the exponent of the Gaussian function. These additional terms, although they improve the fit to the beam frequency spectra, are found not to affect the final physics results significantly.

The center of mass energy distribution $G(E_{cm})$ is obtained from the beam frequency spectrum using Eq. 13 and the relation:

$$E_{cm}^2 = 2m_p^2(1 + \frac{1}{\sqrt{1 - f^2L^2/c^2}}), \tag{28}$$

with L and η determined by the methods described earlier. The measured number of events at the ith point n_i is fitted to the expected number ν_i, given by:

$$\nu_i = \mathcal{L}_i(\sigma_{bkg} + \epsilon\sigma(E_{cm,i})), \tag{29}$$

where $\sigma(E_{cm})$ is the cross section given by Eq. (2), and σ_{bkg} is an estimate of the background cross section. σ_{BW} in Eq. (2) has been modified to include the effect of bremsstrahlung of the initial $\bar{p}p$ state[28]. This effect, although small, decreases the width Γ_R of J/ψ and ψ' by about 10 keV and 2 keV respectively. The resonance mass M_R is not affected. For the J/ψ, the interference between the resonant amplitude and the continuum amplitude for $\bar{p}p \rightarrow e^+e^-$[29] is also considered, but is found not to change the results significantly. The determination of the background for the resonance-fitting procedure is as follows. In the region of the J/ψ and the ψ' resonances the background is so small that the resonance scans, in themselves, cannot determine it. σ_{bkg} is therefore determined from the off-resonance runs and is used as an input to the fitting procedure. The magnitude of the background at J/ψ and ψ' is about 10 pb.

The likelihood function Λ for N data points is calculated as the product of N Poisson functions which give the probability for the ith datum point that n_i events are observed, when ν_i events are expected:

$$\Lambda = \prod_{i=1}^{N} \frac{\nu_i^{n_i} e^{-\nu_i}}{n_i!}. \tag{30}$$

The log-likelihood function $\ln(\Lambda)$ is maximized by varying the parameters, M_R, Γ_R and σ_{peak}. For the double-scan analysis η is also a fit parameter.

VII. RESULTS

The mass of the J/ψ is measured using data from the three 1990 scans. The widths and the branching ratios are determined from the double scans taken in 1990 and 1991. We do not use the 1991 data in the mass determination of the J/ψ because the beam orbit at the J/ψ is very different from the reference orbit at the ψ', and this introduces a large systematic error in the measurement.

The mass of J/ψ and the total width of ψ' have been published earlier[30]. The results in this section supersede those of the previous publication.

A. Determination of the J/ψ Mass

As explained earlier in Sec. IV B, the orbit length is determined by normalizing the result of our measurement for the resonance energy of the ψ' to the known mass[14] $M_R(\psi')$=3686.00±0.10 MeV/c^2. The ψ' mass uncertainty results in the reference orbit length error of ±0.67 mm, which leads to a systematic error of ±0.033 MeV/c^2 in the J/ψ mass. The BPM data are used only to determine ΔL. They contribute a random error of ±1 mm in ΔL, which corresponds to ±0.05 MeV/c^2 at the J/ψ . The error from the fit to the excitation curve, which is due to the event statistics, ranges from 0.009 to 0.012 MeV/c^2, and is combined in quadrature with the BPM error to give the overall statistical uncertainty in the mass measurement. In Table IV we list the resonance mass M_R determined for each of the three scans for J/ψ. We note that the RMS variation of the three values for the resonance mass is 0.045 MeV/c^2, which is entirely consistent with the errors described above, giving further support that the BPM error is estimated correctly. Figure 7 shows the excitation curves for the J/ψ. We obtain for the mass of the J/ψ the value $3096.87 \pm 0.03(stat.) \pm 0.03(sys.)$ MeV/c^2 from the three scans of 1990. This result is an improvement over earlier measurements[2][14].

The same analysis can be used to determine the ψ' mass from the data of the three scans of this resonance taken in 1990. In this case the known J/ψ mass[14] $M_R(J/\psi)$=3096.93±0.09 MeV/c^2 is used as the reference. The J/ψ mass uncertainty of ±0.09 MeV/c^2 corresponds to a reference orbit length error of ±1.8 mm, which leads to a systematic error of ±0.27 MeV/c^2 in the ψ' mass. The ±1 mm error in ΔL due to the BPM corresponds to ±0.15 MeV/c^2 at the ψ'. The error from the fit to the excitation curve ranges from 0.02 to 0.03 MeV/c^2. The RMS variation of the three values for the ψ' mass is 0.183 MeV/c^2, which is also consistent with the errors described above. Figure 8 shows the excitation curves for the ψ'. We obtain for the mass of the ψ' the value $3686.02 \pm 0.09(stat.) \pm 0.27(sys.)$ MeV/c^2. This result is less accurate than earlier measurements[2][14].

Since these six scans are scattered throughout the run, the small variation of the obtained values for the resonance masses is also evidence for the long term stability of our experimental apparatus.

B. Determination of Resonance Widths and Branching Ratios

As mentioned earlier, an independent determination of the width Γ_R (as opposed to the product $\sigma_{peak}\Gamma_R$) is possible with our beam even for the narrow states J/ψ and ψ'. Our approach differs from the one used in the case of e^+e^- measurements of the J/ψ and the ψ', where $\Gamma_B \approx 2.5$ MeV, which precludes any shape analysis of the excitation curve. The beam width in our case is determined with good precision by the double scan technique. The double scan excitation curves are plotted in Figs. 9 and 10. Resonance parameters and η obtained from a fit are listed in Tables V and II, where the errors shown are only the statistical errors due to event statistics as determined by the fitting program.

The measurement of Γ_R does not depend on the absolute value of E_{cm}; only the relative value of E_{cm} is needed. Thus only the orbit length change from data point to data point is relevant in determining the error of Γ_R. This variation can be estimated by two methods. First, the orbit length difference of each side and central orbit pair,

$$L_c - L_s = \frac{L_c}{\eta\gamma_t^2}\frac{f_c - f_s}{f_c}, \tag{31}$$

can be calculated directly from the data. The RMS variation of L_c (or L_s) is $1/\sqrt{2}$ of the RMS variation in $L_c - L_s$, and is found to be ≈ 0.4 mm (≈ 0.2 mm) for the J/ψ (ψ'). Systematic errors in L_c (or L_s) due to the magnet power supply digital setting error and to magnet ramp non-linearity are calculated to be 0.027 mm and less than 0.05 mm respectively. The second method of determining the variation in the orbit length uses the orbit length calculated from the BPM data. For the 1991 data, the two methods give consistent results. For the 1990 data, the second method is not used because the BPM least significant bit was not small enough to resolve this small orbit length variation. The equivalent Γ_R error due to the orbit length variation is then calculated using a Monte Carlo method. In this calculation the energy of each data point is smeared by the energy uncertainty due to the orbit length variation, and a width is determined using the smeared energy; the variations in the width over many trials are used to estimate the error in Γ_R. We obtain an uncertainty of 4 and 24 keV due to this effect for the J/ψ and the ψ' respectively, which is added in quadrature with the statistical error of the fit to obtain the total statistical error.

The systematic error is primarily caused by the fact that the beam energy width decreases continuously[1] as the circulating beam intensity decreases during the data

---

[1] This is due to the fact that the stochastic cooling rate is inversely proportional to the beam intensity. For the excitation curves shown in this paper (Fig. 7, 8, 9 and 10) each data point has been rescaled to the average Γ_B for the data shown in each figure.

taking of a scan. Different methods of averaging and parameterizing the beam revolution frequency spectra taken at each energy data point have been tried and a range of fitted Γ_R has been determined. We use this range to estimate this systematic error. All other systematic errors are small compared to this one. We obtain Γ_R to be $99 \pm 12(stat.) \pm 6(sys.)$keV for the J/ψ and $306 \pm 36 \pm 16$keV for the ψ' after averaging the two scans for each resonance. These values are larger than the earlier measured values from e^+e^- colliding beam experiments[14][31], but agree with them within the quoted errors.

Our results for Γ_R and $B_{in}B_{out}$ obtained from averaging the two double scans for each resonance are summarized in Table VI. $B_{in}B_{out}$ stands for the product $B(J/\psi \to \bar{p}p)\ B(J/\psi \to e^+e^-)$ in the case of the J/ψ, and for the product $B(\psi' \to \bar{p}p)\ [B(\psi' \to e^+e^-) + B(\psi' \to J/\psi X)B(J/\psi \to e^+e^-)]$ for the ψ'. The errors shown in the table are statistical and systematic in that order.

The total statistical error for $B_{in}B_{out}$ is the sum of the uncertainty in the efficiency (Table III) and the error from the fit, which is due to the event statistics, added in quadrature. $B_{in}B_{out}$ and Γ_R are strongly correlated; the product of the two is constrained by the area (see Eqs. 2 and 3). The systematic error in $B_{in}B_{out}$ is the sum in quadrature of the contribution due to the systematic error in Γ_R, and the error due to the luminosity measurement ($\pm 4\%$, see Sec. V).

We can calculate the branching ratios $B(J/\psi \to \bar{p}p)$ and $B(\psi' \to \bar{p}p)$ if we use the branching ratios $B(J/\psi \to e^+e^-)$, $B(\psi' \to e^+e^-)$ and $B(\psi' \to J/\psi X)$ from Ref. [14]. These values are also shown in Table VI. The three errors shown in the table for $B(J/\psi \to \bar{p}p)$, and $B(\psi' \to \bar{p}p)$ are statistical, systematic, and the error due to the uncertainties in the published values for the branching ratios ($B(J/\psi \to e^+e^-)$, $B(\psi' \to e^+e^-)$ and $B(\psi' \to J/\psi X)$) respectively.

Our results for the product $A^* = \Gamma_R B_{in}B_{out}$, which is proportional to the area (see Eqs. 2 and 3), can be compared with values obtained from e^+e^- experiments[14]. We find for the J/ψ that $A^*_{J/\psi} = 11.3 \pm 0.6$ eV, to be compared with 11.6 ± 0.9 eV (all errors are added in quadrature). For the ψ' we obtain $A^*_{\psi'} = 3.6 \pm 0.2$ eV which is larger than 2.1 ± 0.6 eV, the value derived from e^+e^- experiments.

ACKNOWLEDGMENTS

The authors wish to acknowledge the help of the members of the Fermilab Accelerator Division. We also wish to thank the staff, engineers, and technicians at our respective institutions for their help and cooperation. We wish to thank in particular L. Bartoszek, C. Chizzo, E. Hahn, E. Harms, C. Kendziora, H. Koecher, D. McGinnis, J. Sasek, J. Western (Fermilab), S. Bigoni, G. Bonora, V. Carassiti, G. Sorrentino, L. Tracchi (Ferrara), R. Tilden (Northwestern), G. Barisone, S. Minutoli, M. Negri, P. Poggi, A. Pozzo (Genoa), J. Passaneau (Penn State), G. Algostino, F. Bertolino, F. Callá, D. Dattola, G. Dughera, R. Farano, G. Giraudo (Turin). Useful discussions with, and the support of J. Marriner (Fermilab) are also gratefully acknowledged.

This research was supported in part by the U.S. Department of Energy, the U.S.

National Science Foundation and the Istituto Nazionale di Fisica Nucleare of Italy.

* Now at Fermi National Accelerator Laboratory, Batavia, Illinois 60510.

† Now at CEN Saclay, F-91191 Gif-sur-Yvette, France.

[1] For a review of the early e^+e^- experiments, see G.J.Feldman and Martin L.Perl, Phys. Rep. **33C**, 285 (1977).

[2] A. A. Zholentz *et al.,* Phys. Lett. B **96**, 214 (1980).

[3] P. Dalpiaz, in *Proceedings of the first LEAR workshop*, Karlsruhe, Germany, edited by H. Poth (Kernforschungszentrum Karlsruhe, 1979).

[4] T. A. Armstrong *et al.,* Report No. FERMILAB-Pub-92/186-E, July 1992, submitted to Phys. Rev. Lett.

[5] M. Macrí, in *Antiprotons for colliding beam facilities: Proceedings of the 1983 CERN Accelerator School*, edited by P. Bryant and S. Newman (CERN 84-15, 1984), p. 469.

[6] C. Baglin *et al.,* Nucl. Phys. B **286**, 592 (1987).

[7] Design Report: Tevatron I Project, Fermi National Accelerator Laboratory, Batavia, Illinois (unpublished), Sept. 1984.

[8] J. Peoples, Jr., in *Proceedings of the Workshop on the Design of a Low Energy Antimatter Facility*, edited by D. Cline, (World Scientific Publishing Co, Singapore, 1986), p. 144.

[9] V. Bharadwaj *et al.,* in *Proceedings of the European Particle Accelerator Conference,* Rome, edited by S. Tazzari, (World Scientific Publishing Co, Singapore, 1989), p. 964.

[10] For a review, see D. Möhl, G. Petrucci, L. Thorndahl, and S. van der Meer, Phys. Rep. **58**, 73 (1980).

[11] J. Petter, D. McGinnis, J. Marriner, and J. Misek, in *Proceedings of the 1989 IEEE Particle Accelerator Conference,* Vol. 1, 648 (1989).

[12] For an introduction to Schottky noise properties, see S. Chattopadhyay, in *Proceedings of Physics of High Energy Accelerators*, edited by Melvin Month, Per F. Dahl and Margaret Dienes, (AIP Conference Proceedings No. 127, New York, 1985).

[13] *Hewlett Packard 8568B Spectrum Analyzer Operating and Programming Manual,* Hewlett-Packard Co., Rohnert Park, California 94928, 1984.

[14] Particle Data Group, "Review of Particle Properties," Phys. Rev. D **45**, S1 (1992).

[15] T. Bagwell, S. Holmes, J. McCarthy, and R. Weber, "*Antiproton Source Beam Position System,*" Fermilab Technical Memo 1254, Batavia, Illinois (unpublished), May 1984.

[16] E.D. Courant and H.S. Snyder, Ann. Phys. (N. Y.) **3**, 1 (1958).

[17] C. Biino *et al.,* Nucl. Instrum. Methods **A317**, 135 (1992).

[18] L. Bartoszek *et al.*, Nucl. Instrum. Methods **A301**, 47 (1991).
[19] R. Ray *et al.*, Nucl. Instrum. Methods **A307**, 254 (1991).
[20] M. A. Hasan *et al.*, Nucl. Instrum. Methods **A295**, 73 (1990).
[21] C. Biino *et al.*, Nucl. Instrum. Methods **A271**, 417 (1988); IEEE Trans. Nucl. Sci. **36**, 98 (1989).
[22] R. Calabrese *et al.*, Nucl. Instrum. Methods **A277**, 116 (1989).
[23] G. Barisone *et al.*, Report No. Genova INFN/AE-89, 1989 (unpublished).
[24] M. Sarmiento *et al.*, *"A Luminosity Monitor for FNAL experiment E760,"* to be submitted to Nucl. Instrum. Methods.
[25] T. A. Armstrong *et al.*, Nucl. Phys. B **373**, 35 (1992).
[26] L. Köpke and N. Wermes, Phys. Rep. **174C**, 67 (1989).
[27] L. S. Brown and R. N. Cahn, Phys. Rev. Lett. **35**, 1, (1975).
[28] D. C. Kennedy, Phys. Rev. D **46**, 461 (1992).
[29] T. A. Armstrong *et al.*, Report No. FERMILAB-Pub-92/244-E, September 1992, to be submitted to Phys. Rev. Lett.
[30] T. A. Armstrong *et al.*, Phys. Rev. Lett. **68**, 1468 (1992).
[31] S. Y. Hsueh and S. Palestini, Phys. Rev. D **45**, 2181 (1992).

FIGURES

FIG. 1. Layout of one sector of the Accumulator lattice. The solid line is β_x, the dashed line is β_y, and the dash-dot line is the dispersion.

FIG. 2. Sample longitudinal Schottky spectra at harmonic number $h = 129$. Note the logarithmic scale (in dB) for the vertical axis. (a) Data taken in 1990 at the J/ψ fitted to a double Gaussian with exponential tails. (b) Data taken in 1991 at the J/ψ fitted to a Gaussian with an 8th order polynomial added to the exponent and exponential tails.

FIG. 3. Schematic for the sequence of the double scan.

FIG. 4. Layout of the detector and gas jet.

FIG. 5. Invariant mass distribution of electron pairs for the 1991 J/ψ scan (open area) and for the off-resonance background normalized to the same luminosity(shaded area). The level of background has been multiplied by a factor of 10 to make it discernible.

FIG. 6. Invariant mass distribution of electron pairs for the 1991 ψ' scan (open area) and for the off-resonance background normalized to the same luminosity (shaded area).

FIG. 7. Excitation curves for J/ψ. Data from the first 1990 single scan are shown as crosses, from the second 1990 single scan as diamonds, and from the 1990 double scan as squares.

FIG. 8. Excitation curves for ψ'. Data from the first 1990 single scan are shown as crosses, from the second 1990 single scan as diamonds, and from the 1990 double scan as squares.

FIG. 9. 1991 J/ψ double scan. The x-axis is the invariant mass of the *central orbit.* The lines are theoretical excitation curves calculated using the best fit parameters.

FIG. 10. 1991 ψ' double scan. The x-axis is the invariant mass of the *central orbit.* The lines are theoretical excitation curves calculated using the best fit parameters.

TABLES

TABLE I. Charmonium states and the corresponding beam energy of an antiproton beam for $p\bar{p}$ resonant production.

State	J^{PC}	Mass (MeV/c^2)	E_{beam} (MeV)
η_c	0^{-+}	2979.6	3792.8
J/ψ	1^{--}	3096.9	4172.6
χ_{c0}	0^{++}	3415.1	5276.8
χ_{c1}	1^{++}	3510.6	5629.3
$h_c(^1P_1)$	1^{+-}	3526.2	5687.8
χ_{c2}	2^{++}	3556.3	5801.4
η_c'	0^{-+}	3594.0	5945.0
ψ'	1^{--}	3686.0	6301.9
$^1D_2$	2^{-+}		
$^3D_2$	2^{--}		

TABLE II. η measured by three methods

Data	double scan	synchrotron frequency[a]	γ_t
J/ψ 1990	0.020 ± 0.001	0.0185	0.0186
J/ψ 1991	0.0181 ± 0.0004	0.0179	
ψ' 1990	-0.0087 ± 0.0005	-0.0105	-0.0109
ψ' 1991	-0.0140 ± 0.0008	-0.0142	-0.0136

[a] The estimated error in η is $\pm 10\%$.

TABLE III. Efficiencies

Data	ϵ_{trig}	ϵ_{anal}	ϵ_{geom}	ϵ
J/ψ 1990	0.85 ± 0.02	0.886 ± 0.013	0.487 ± 0.008	0.358 ± 0.012
J/ψ 1991	0.92 ± 0.02	0.834 ± 0.009	0.487 ± 0.008	0.374 ± 0.011
ψ' 1990	0.82 ± 0.02	0.813 ± 0.011	0.527 ± 0.023	0.351 ± 0.018
ψ' 1991	0.88 ± 0.02	0.833 ± 0.011	0.527 ± 0.023	0.386 ± 0.020

TABLE IV. J/ψ mass measurements

Data	J/ψ Mass(MeV/c^2)[a]
1990 single scan 1	$3096.898 \pm 0.051 \pm 0.033$
1990 single scan 2	$3096.816 \pm 0.051 \pm 0.033$
1990 double scan	$3096.902 \pm 0.051 \pm 0.033$
Average	$3096.87 \pm 0.03 \pm 0.03$

[a] The errors are statistical and systematic, respectively.

TABLE V. J/ψ and ψ' double scan fit results[a]

Data	Width(keV)	$B_{in}B_{out}$
J/ψ 1990	89 ± 23	$(1.18^{+0.43}_{-0.22}) \times 10^{-4}$
J/ψ 1991	103 ± 15	$(1.13^{+0.17}_{-0.14}) \times 10^{-4}$
ψ' 1990	310 ± 49	$(1.23^{+0.21}_{-0.17}) \times 10^{-5}$
ψ' 1991	302 ± 42	$(1.13^{+0.18}_{-0.13}) \times 10^{-5}$

[a] The errors shown are due solely to event statistics.

TABLE VI. J/ψ and ψ' final results

Resonance	Width(keV)	$B_{in}B_{out}$[a]	$B(\bar{p}p)$[b]
J/ψ	$99 \pm 12 \pm 6$	$(1.14^{+0.16}_{-0.12} \pm 0.10) \times 10^{-4}$	$(1.82^{+0.26}_{-0.19} \pm 0.16 \pm 0.06) \times 10^{-3}$
ψ'	$306 \pm 36 \pm 16$	$(1.17^{+0.14}_{-0.12} \pm 0.08) \times 10^{-5}$	$(2.61^{+0.31}_{-0.27} \pm 0.17 \pm 0.17) \times 10^{-4}$

[a] $B_{in}B_{out} = B(J/\psi \to \bar{p}p)\ B(J/\psi \to e^+e^-)$ for the J/ψ, and
$B_{in}B_{out} = B(\psi' \to \bar{p}p)\ [B(\psi' \to e^+e^-) + B(\psi' \to J/\psi X)B(J/\psi \to e^+e^-)]$ for the ψ'.
The errors, in the order shown, are statistical and systematic.

[b] Using $B(J/\psi \to e^+e^-)$, $B(\psi' \to e^+e^-)$, and $B(\psi' \to J/\psi + X)$ from Ref. [14].
The errors, in the order shown, are statistical, systematic, and due to the errors in the branching ratios from Ref. [14].

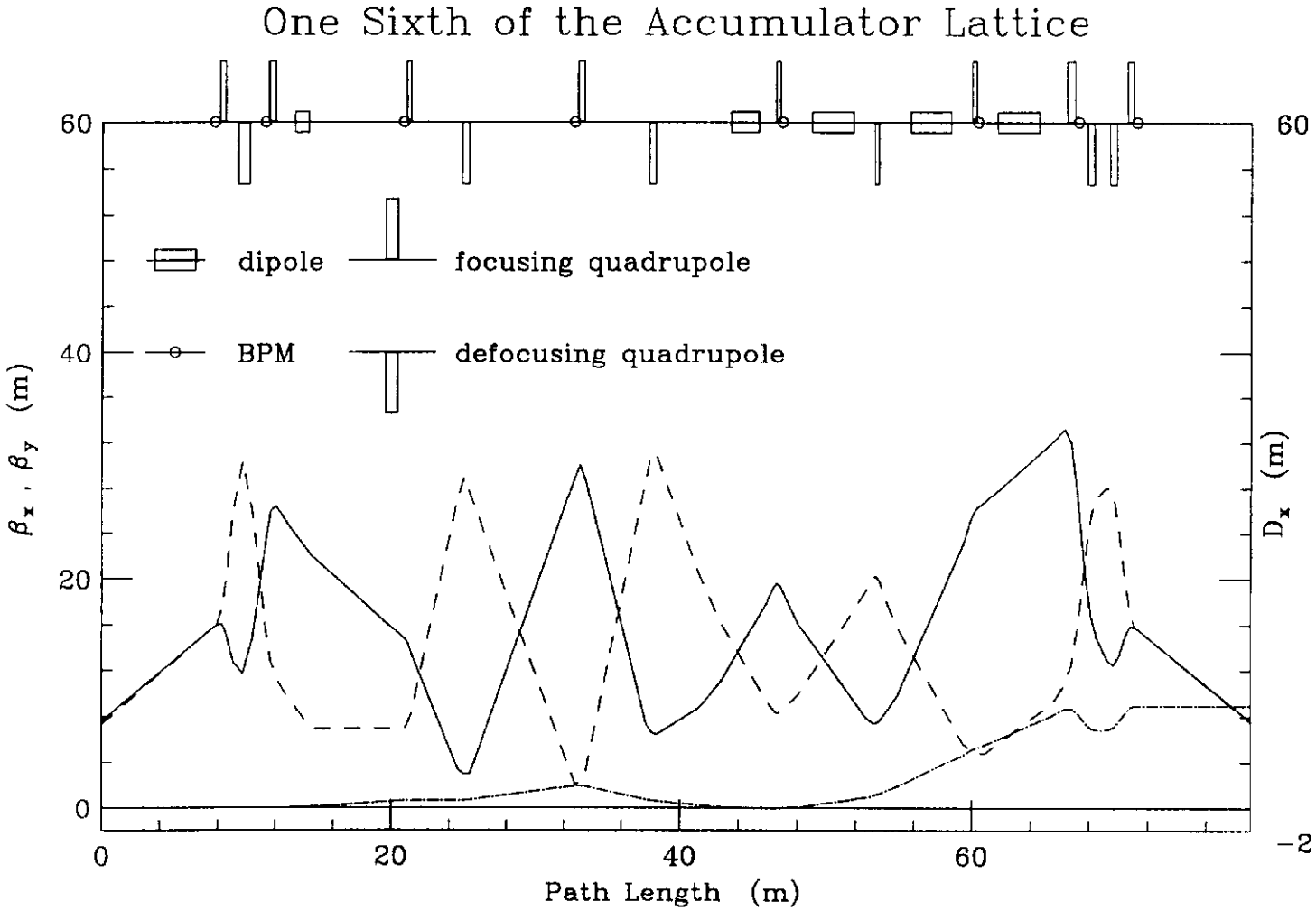

FIG. 1. Layout of one sector of the Accumulator lattice. The solid line is β_x, the dashed line is β_y, and the dash-dot line is the dispersion.

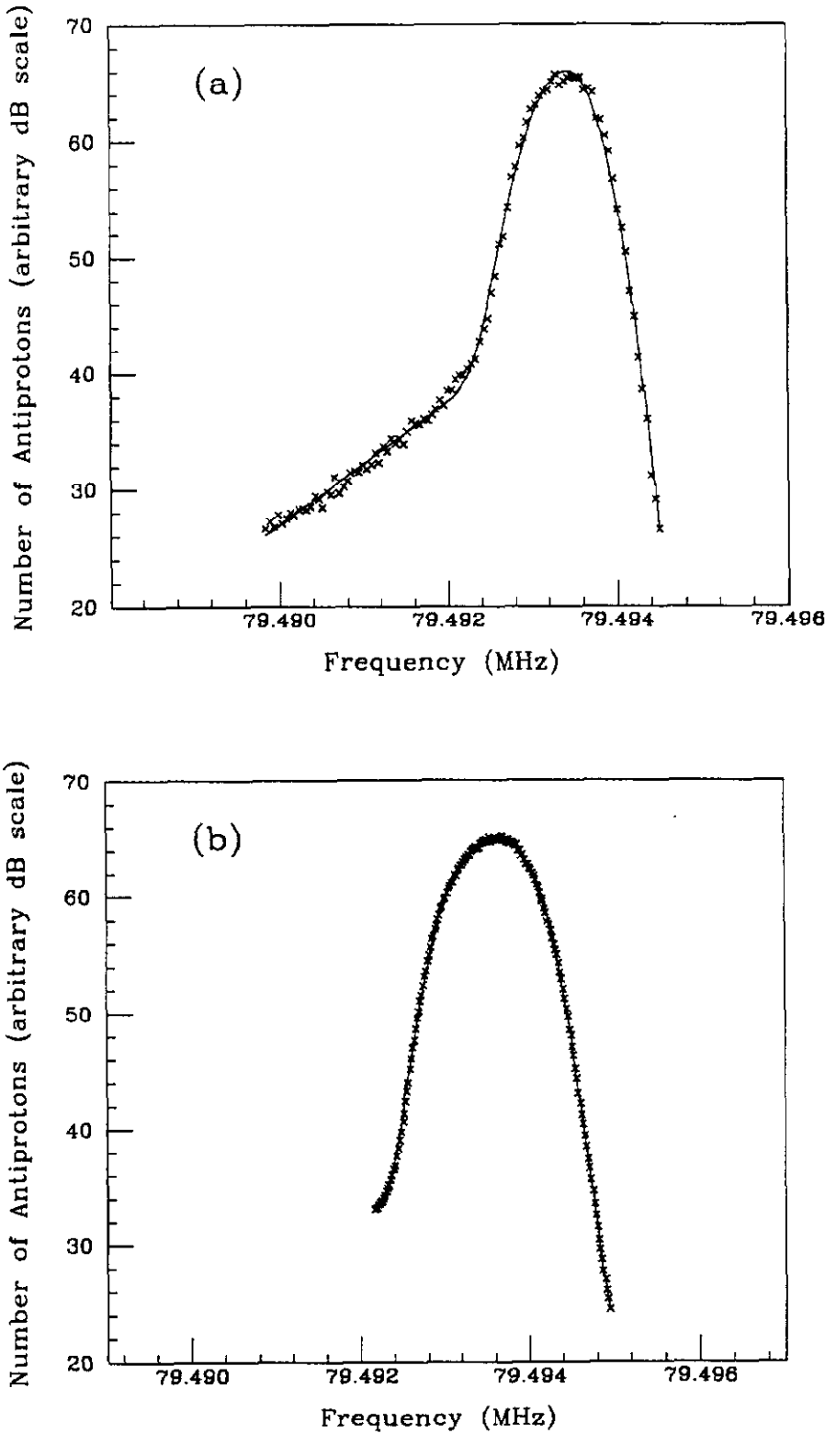

FIG. 2. Sample longitudinal Schottky spectra at harmonic number $h = 129$. Note the logarithmic scale (in dB) for the vertical axis. (a) Data taken in 1990 at the J/ψ fitted to a double Gaussian with exponential tails. (b) Data taken in 1991 at the J/ψ fitted to a Gaussian with an 8th order polynomial added to the exponent and exponential tails.

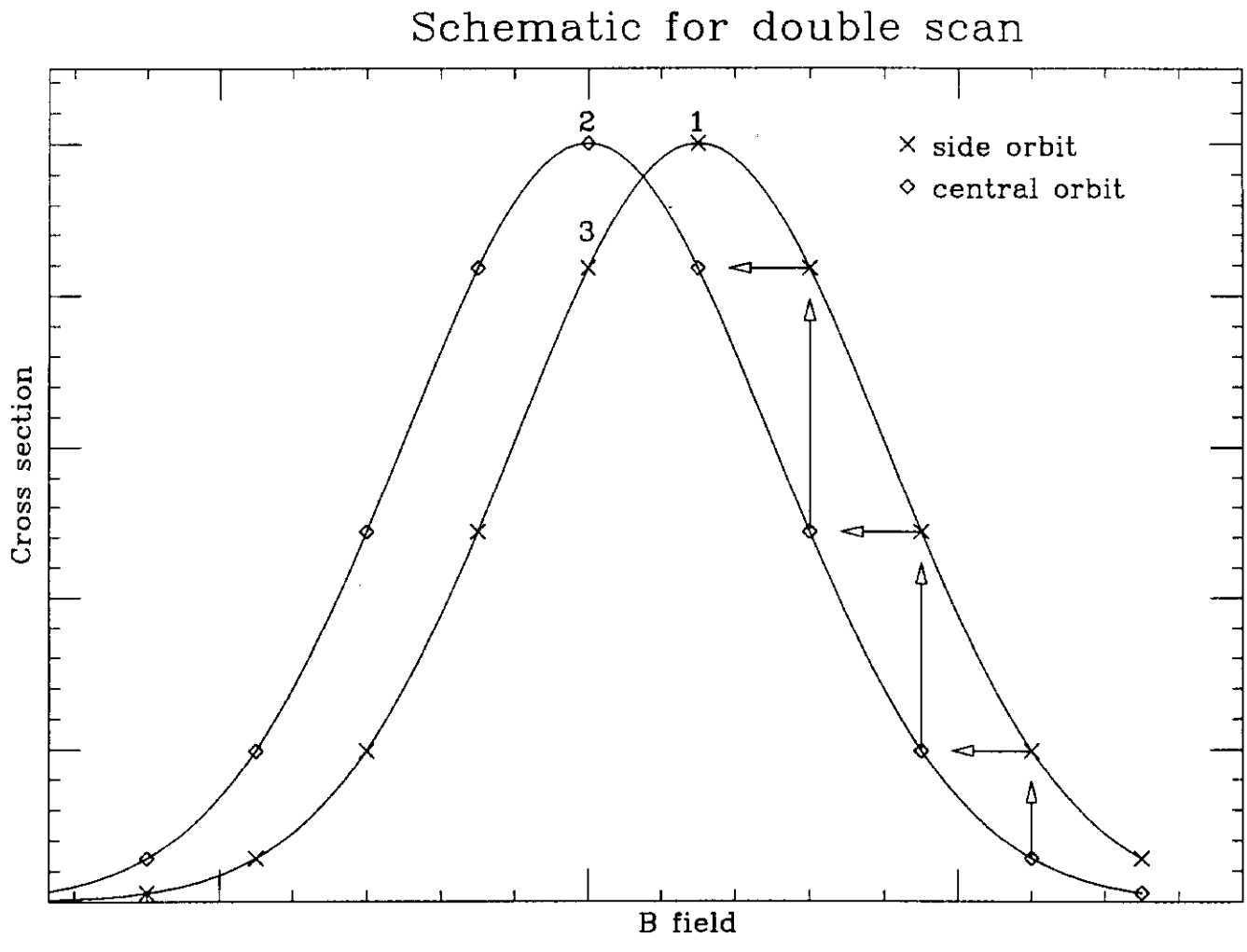

FIG. 3. Schematic for the sequence of the double scan.

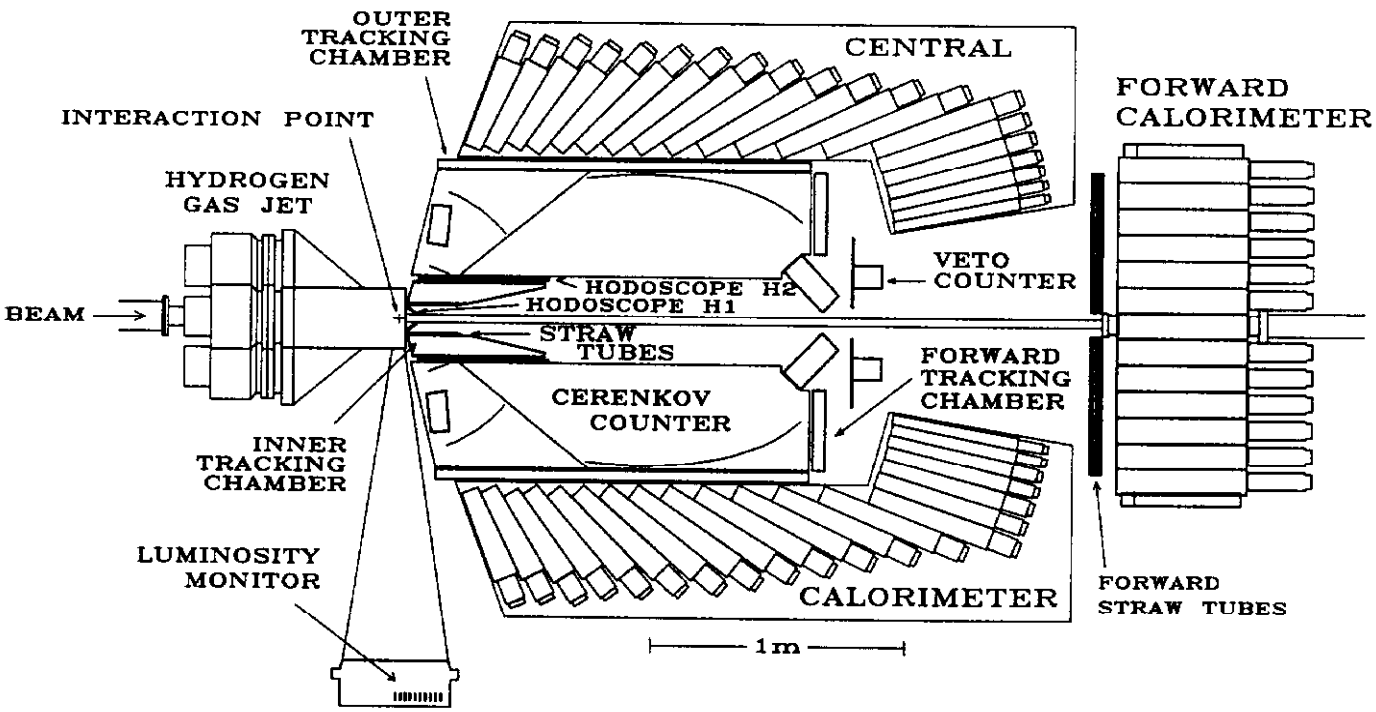

FIG. 4. Layout of the detector and gas jet.

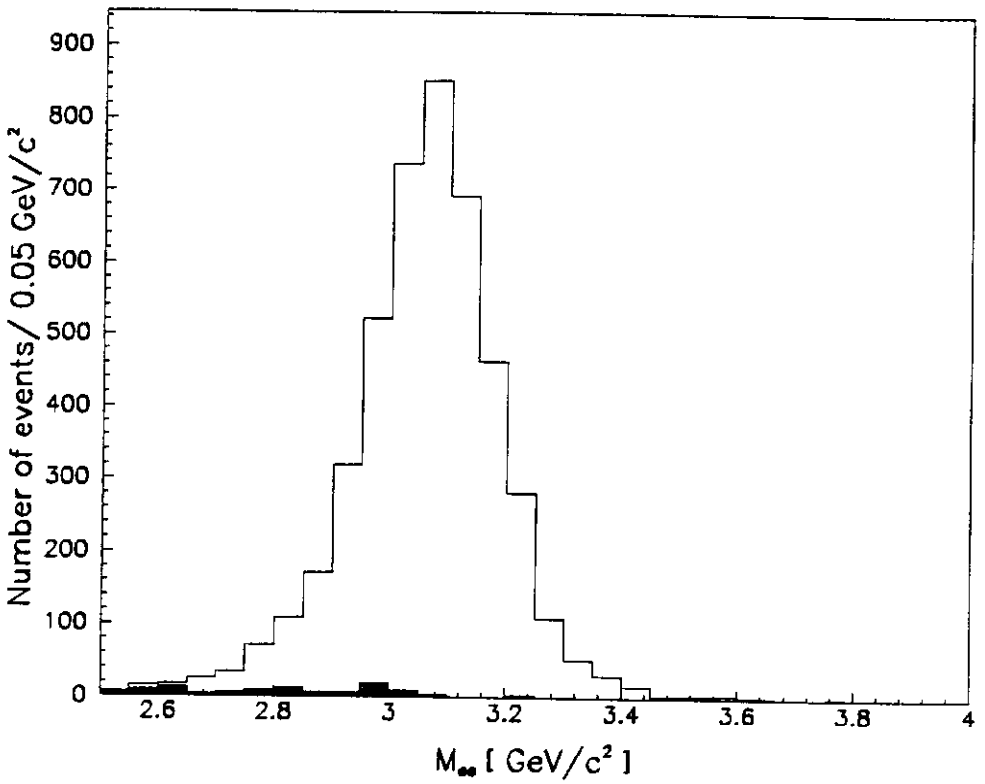

FIG. 5. Invariant mass distribution of electron pairs for the 1991 J/ψ scan (open area) and for the off-resonance background normalized to the same luminosity(shaded area). The level of background has been multiplied by a factor of 10 to make it discernible.

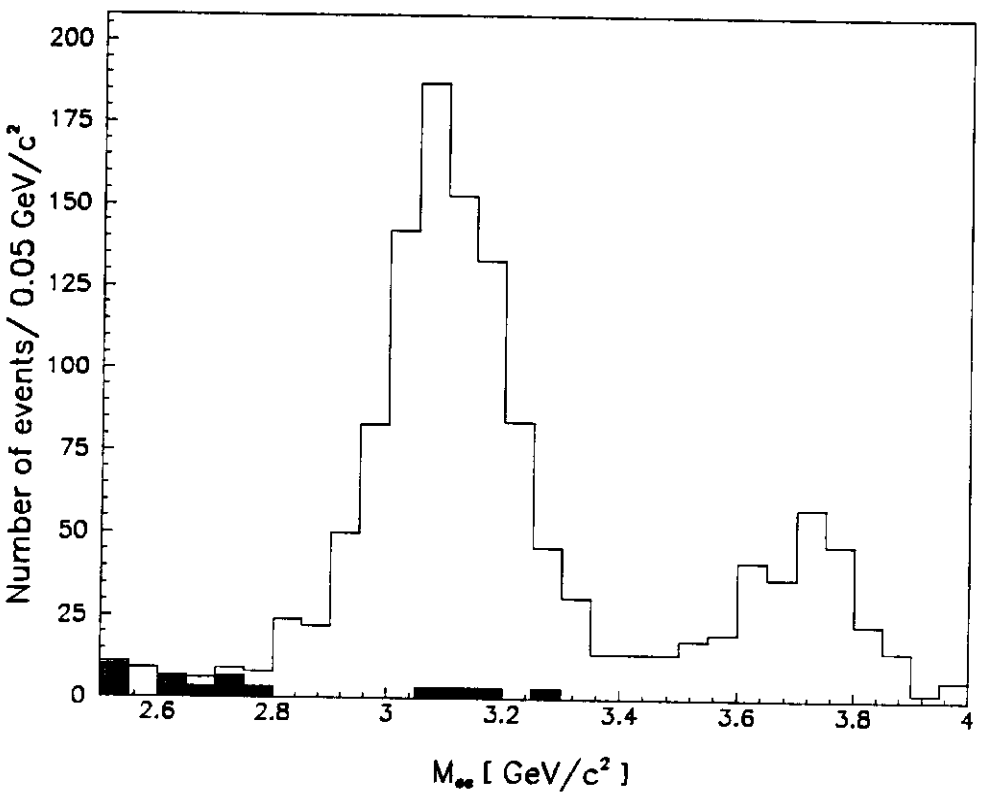

FIG. 6. Invariant mass distribution of electron pairs for the 1991 ψ' scan (open area) and for the off-resonance background normalized to the same luminosity (shaded area).

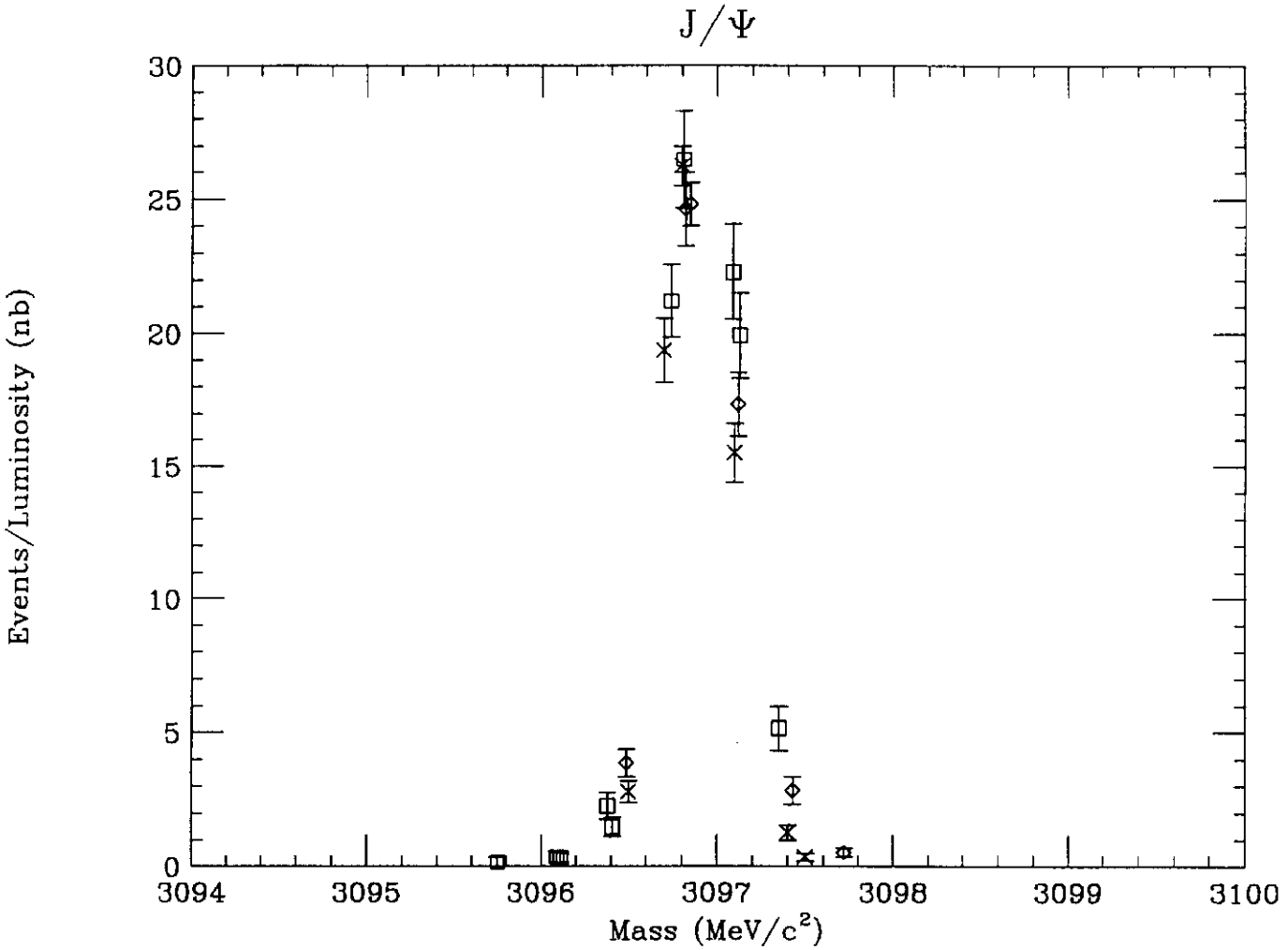

FIG. 7. Excitation curves for J/ψ. Data from the first 1990 single scan are shown as crosses, from the second 1990 single scan as diamonds, and from the 1990 double scan as squares.

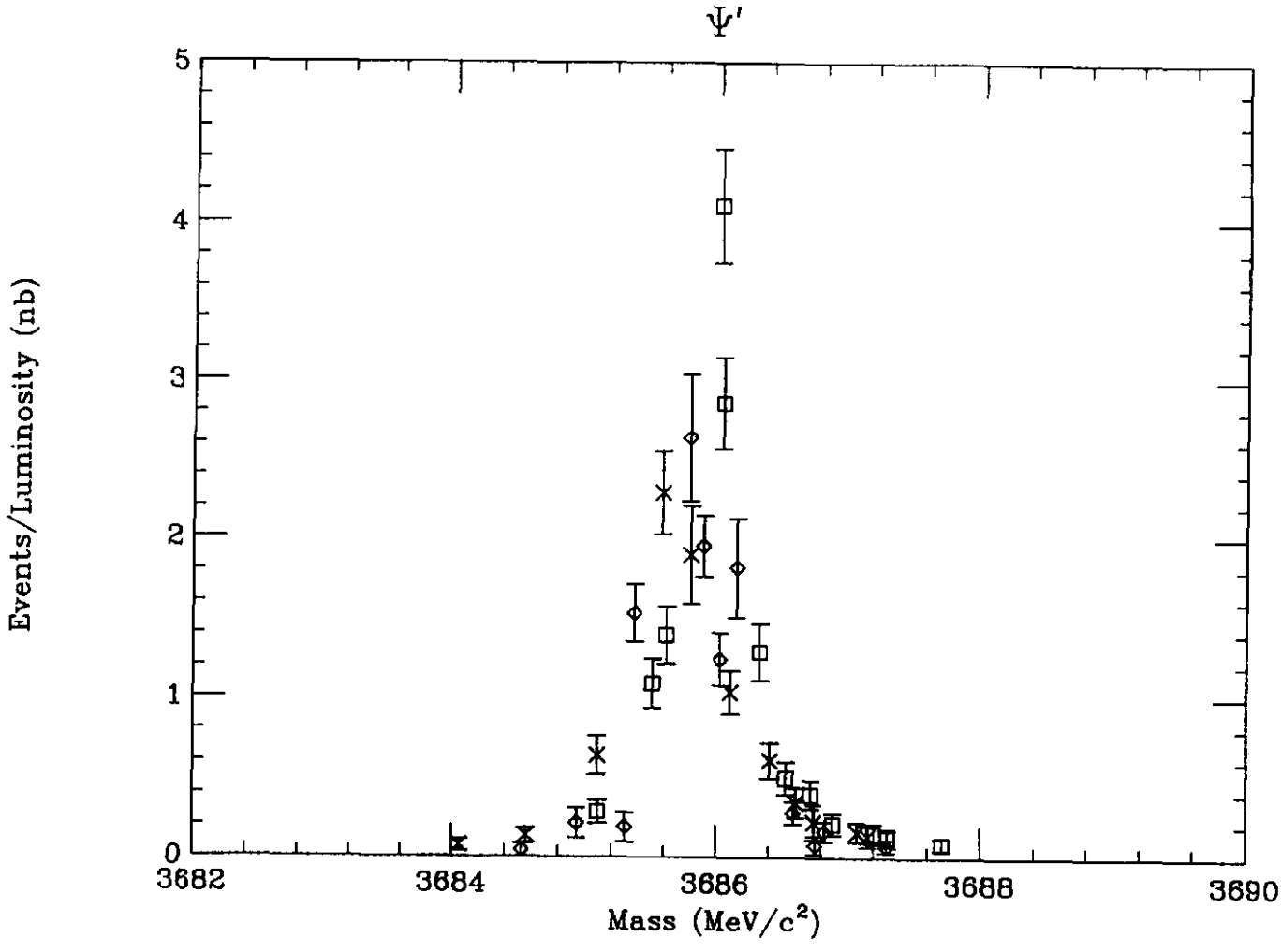

FIG. 8. Excitation curves for ψ'. Data from the first 1990 single scan are shown as crosses, from the second 1990 single scan as diamonds, and from the 1990 double scan as squares.

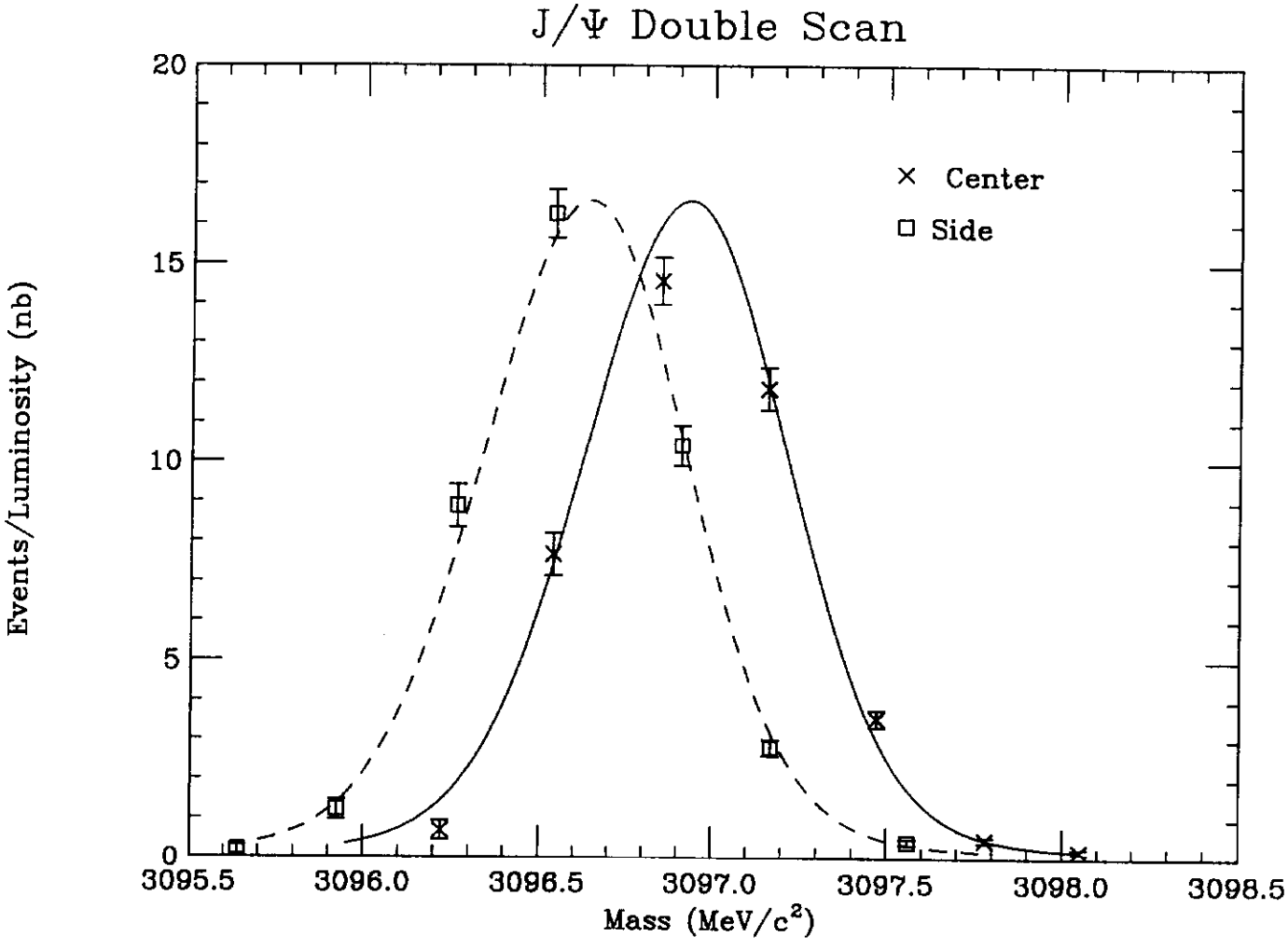

FIG. 9. 1991 J/ψ double scan. The x-axis is the invariant mass of the *central orbit.* The lines are theoretical excitation curves calculated using the best fit parameters.

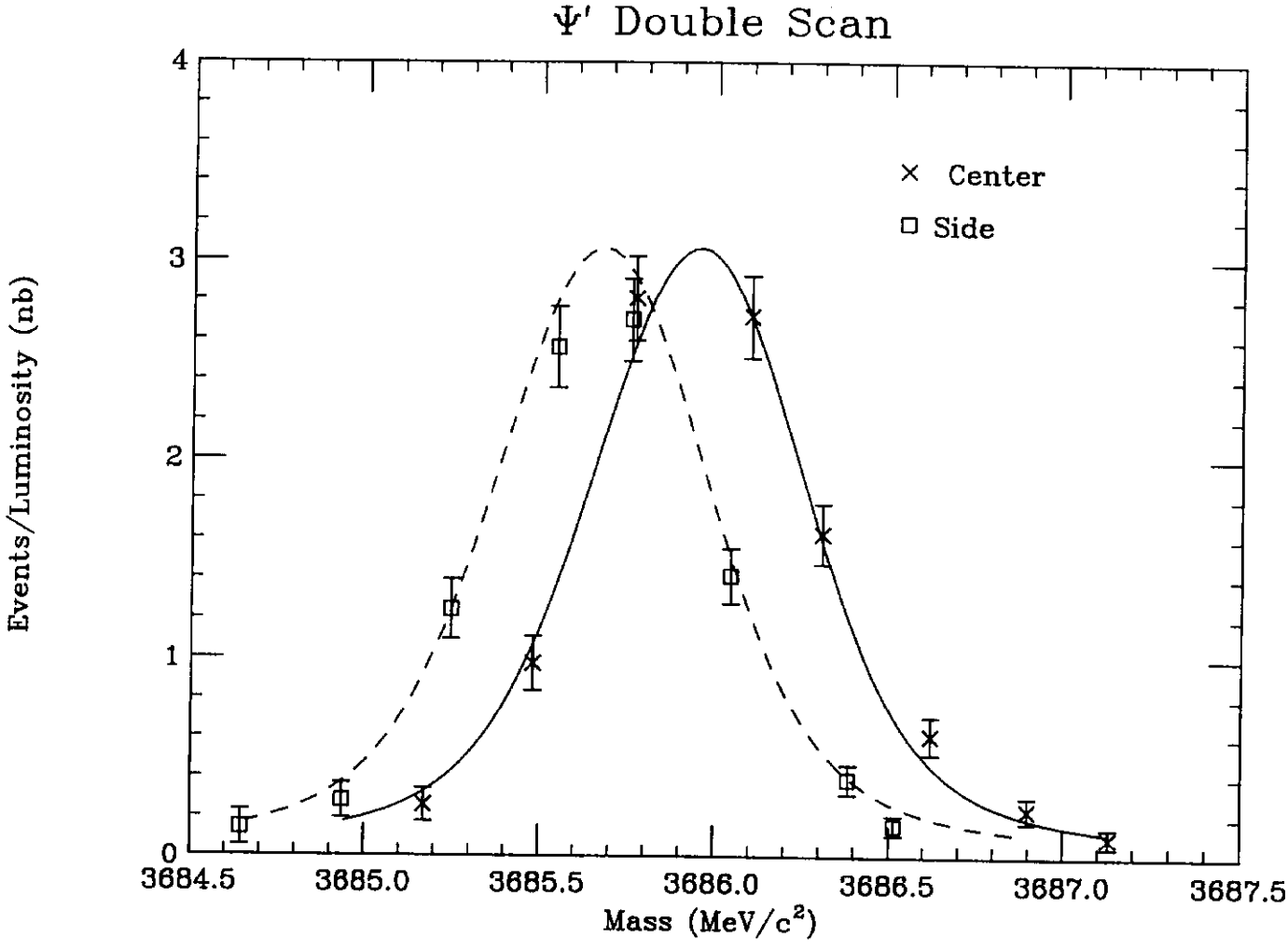

FIG. 10. 1991 ψ' double scan. The x-axis is the invariant mass of the *central orbit*. The lines are theoretical excitation curves calculated using the best fit parameters.